The response of beam and slab bridges to moving forces

Autor(en): **Iyengar, K.T. Sundara Raja / Jagadish, K.S.**

Objekttyp: **Article**

Zeitschrift: **IABSE publications = Mémoires AIPC = IVBH Abhandlungen**

Band (Jahr): **28 (1968)**

PDF erstellt am: **23.07.2024**

Persistenter Link: https://doi.org/10.5169/seals-22182

The Response of Beam and Slab Bridges to Moving Forces

Comportement de ponts-dalles sous charges mobiles

Verhalten von Platten- und Balkenbrücken unter beweglichen Lasten

K. T. SUNDARA RAJA IYENGAR
Professor of Civil Engineering

K. S. JAGADISH
Lecturer in Civil Engineering

Indian Institute of Science, Bangalore – 12, India

Introduction

The dynamic response of a Highway bridge under moving loads is usually studied by treating the bridge as a beam. Such a treatment would be satisfactory if the span/width ratio of the bridge is large. It is known that a good majority of the highway bridges may have spans comparable to the widths. For such bridges, the beam theory is not adequate and a suitable two-dimensional theory will have to be adopted to consider the influence of the transverse flexibility of the bridge on its response.

There have been a few publications in the literature, which take the transverse flexibility of the bridge into account while studying its response. ALFARO and VELETSOS [1] have conducted some experimental studies on the response of an aluminium bridge model subjected to a moving sprung load. Later, ORAN and VELETSOS [2] developed an analytical solution to predict the response of the bridge under moving sprung loads, taking the two-dimensional behaviour of the bridge into consideration. In their analysis, the beam and slab highway bridge has been considered as a plate continuous over the beams. Lagrange's equations of motion have been derived and they have been solved numerically using the Newmark-β procedure.

In this paper the beam and slab Highway bridge is analysed as an orthotropic plate simply supported at two opposite edges. The orthotropic plate approximation is often used while studying the static load distribution effects in beam and slab bridges. It is believed that the extension of the orthotropic plate theory to the dynamic bridge problem would be instructive. This approach

is felt to be more convenient for numerical studies than the plate-over-beams analysis used by ORAN and VELETSOS.

The response of a Highway bridge to moving vehicles is usually studied by treating the vehicle as a sprung load. Sometimes the vehicle is also represented by a moving force ignoring its dynamic characteristics. Although the sprung load analysis is more realistic, this paper confines itself to the problem of the bridge under moving force for several reasons. The study of the bridge response under moving force yields useful information on two aspects. Firstly, the study isolates the influence of the speed parameter and secondly it reveals the degree of participation of the various modes in the response.

Analysis

An orthotropic plate bridge simply supported at the edges $x = 0$ and a, and free at the edges $y = \pm b/2$, will now be considered (Fig. 1). A force P is considered to move with uniform velocity "v" in the X-direction along the line $y = c$. P is assumed to be distributed over a square of side $2e$.

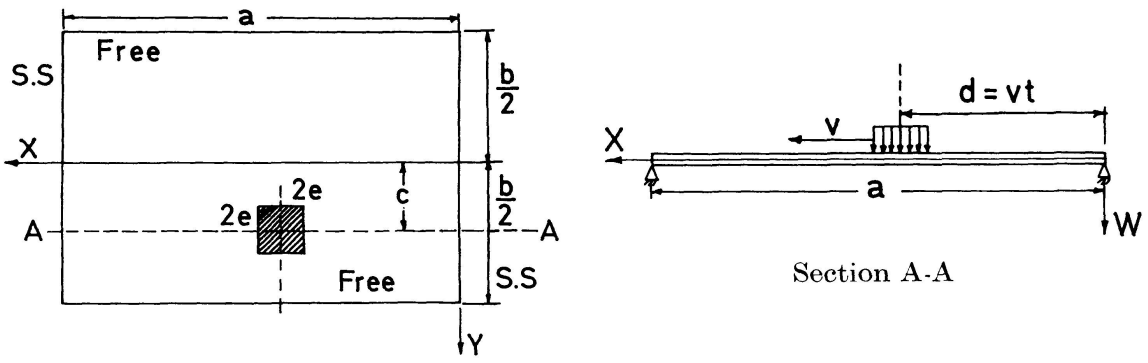

Fig. 1. The orthotropic plate under moving force.

The bridge will be assumed to possess no damping in the following analysis. FOSTER and OEHLER [3] and OEHLER [4] have reported some typical values of damping in actual bridges. Their measurements have shown that the damping values are of the order of 1 per cent of the critical. The neglect of damping appears to be quite reasonable because of the low damping capacity of Highway bridges. The equation of motion of the bridge under the moving force may now be written as

$$D_x \frac{\partial^4 W}{\partial x^4} + 2 H_{xy} \frac{\partial^4 W}{\partial x^2 \partial y^2} + D_y \frac{\partial^4 W}{\partial y^4} + \rho \frac{\partial^2 W}{\partial t^2} = F(x, y, t). \tag{1}$$

D_x, H_{xy} and D_y are the orthotropic plate rigidities and $W(x, y, t)$ is the dynamic deflection of the bridges. $F(x, y, t)$ represents the moving force-distribution function. ρ is the mass per unit area of the bridge. The deflection W will now be separated into two parts:

$$W(x,y,t) = \overline{W}(x,y,t) + U(x,y,t), \tag{2}$$

where $\overline{W}$ satisfies the equation

$$D_x \frac{\partial^4 \overline{W}}{\partial x^4} + 2H_{xy} \frac{\partial^4 \overline{W}}{\partial x^2 \partial y^2} + D_y \frac{\partial^4 \overline{W}}{\partial y^4} = F(x,y,t). \tag{3}$$

$\overline{W}$ represents the deflection of an orthotropic plate whose mass is neglected, under the action of a moving force P. This deflection can be obtained by static analysis and is dependent only on the position of the moving force on the bridge and not on its speed. $\overline{W}$ will be referred to as the "crawl solution".

Combining Eqs. (1), (2) and (3),

$$D_x \frac{\partial^4 U}{\partial x^4} + 2H_{xy} \frac{\partial^4 U}{\partial x^2 \partial y^2} + D_y \frac{\partial^4 U}{\partial y^4} + \rho \frac{\partial^2 U}{\partial t^2} = -\rho \frac{\partial^2 \overline{W}}{\partial t^2}. \tag{4}$$

It may be observed that it is easier to solve Eqs. (3) and (4) separately, than the composite Eq. (1). The difficulty in solving (1) arises due to the concentration in the force P. Eq. (4) is free from this difficulty since the inertia force $\rho \frac{\partial^2 \overline{W}}{\partial t^2}$ is well distributed over the bridge surface. The problem of the concentration of the force still persists in Eq. (3) but it is handled with far greater convenience since the time dependence of $\overline{W}$ is known beforehand from the time dependence of $F(x,y,t)$. The solution of Eq. (4) does not present any problem. $U(x,y,t)$ will be referred to as the "inertia force solution".

The solutions of Eqs. (3) and (4) will now be obtained by using the characteristic functions of the orthotropic plate. These functions have been studied in detail by SUNDARA RAJA IYENGAR and NARAYANA IYENGAR [5, 6]. The various characteristic functions are presented in Appendix. Let $Y_{mn}(y) \operatorname{Sin} \frac{m\pi x}{a}$ represent the deflection shape of the orthotropic plate in one of its modes. Let p_{mn} be the circular frequency of vibration for the same mode. The orthogonal property of the characteristic functions $Y_{mn} \operatorname{Sin} \frac{m\pi x}{a}$ can be made use of in expanding arbitrary functions by a series of these functions.

The function $F(x,y,t)$ may be defined as

$$F(x,y,t) = \frac{P}{4e^2} \quad \text{if, } d-e<x<d+e \text{ and } c-e<y<c+e,$$

$$= 0 \quad \text{if, } x<d-e \text{ or } >d+e \text{ and } y<c-e \text{ or } >c+e,$$

where $d = vt$.

This function may now be expanded by a double series. The series assumes the form:

$$F(x,y,t) = \sum_{m=1,\ldots}^{\infty} \sum_{n=1,\ldots}^{\infty} b_{mn}(t)\, Y_{mn}(y) \operatorname{Sin} \frac{m\pi x}{a}. \tag{6}$$

Hence,
$$b_{mn}(t) \int_0^a \int_{-b/2}^{+b/2} Y_{mn}^2 \operatorname{Sin}^2 \frac{m\pi x}{a}\, dx\, dy = P \operatorname{Sin} \frac{m\pi v t}{a} f_{mn},$$

where $$f_{mn} = \frac{\operatorname{Sin}\frac{m\pi e}{a}}{\frac{m\pi e}{a}} \frac{1}{2e} \int_{c-e}^{c+e} Y_{mn}\, dy.$$

Putting $$K_{mn}\, a\, b = \int_0^a \int_{-b/2}^{+b/2} Y_{mn}^2 \operatorname{Sin}^2 \frac{m\pi x}{a}\, dx\, dy;$$

$$b_{mn}(t) = \frac{P f_{mn}}{K_{mn}\, a\, b} \operatorname{Sin} \frac{m\pi v t}{a}. \tag{7}$$

Now $\overline{W}(x, y, t)$ may also be expanded by a series in terms of $Y_{mn} \operatorname{Sin}\frac{m\pi x}{a}$.

$$\overline{W}(x, y, t) = \sum_{m=1,\ldots}^{\infty} \sum_{n=1,\ldots}^{\infty} a_{mn}(t)\, Y_{mn} \operatorname{Sin} \frac{m\pi x}{a}. \tag{8}$$

Combining (3), (6) and (8)

$$a_{mn}(t) = \frac{P a^2}{D_x} \frac{a}{b} \frac{f_{mn}}{K_{mn} \lambda_{mn}} \operatorname{Sin} \frac{m\pi v t}{a}, \tag{9}$$

where $$\lambda_{mn} = \frac{\rho\, p_{mn}^2\, a^4}{D_x}.$$

This equation is a consequence of the fact that $Y_{mn} \operatorname{Sin}\frac{m\pi x}{a}$ is a characteristic function of the orthotropic plate. Hence

$$\overline{W} = \frac{P a^2}{D_x} \frac{a}{b} \sum_{m=1,\ldots}^{\infty} \sum_{n=1,\ldots}^{\infty} \frac{f_{mn}}{\lambda_{mn} K_{mn}} \operatorname{Sin} \frac{m\pi v t}{a} Y_{mn} \operatorname{Sin} \frac{m\pi x}{a}. \tag{10}$$

The solution of Eq. (4) may now be taken in the form

$$U(x, y, t) = \sum_{m=1,\ldots}^{\infty} \sum_{n=1,\ldots}^{\infty} q_{mn}(t)\, Y_{mn} \operatorname{Sin} \frac{m\pi x}{a}. \tag{11}$$

Combining Eqs. (4), (10) and (11),

$$\ddot{q}_{mn} + p_{mn}^2 q_{mn} = \frac{P a^2}{D_x} \frac{a}{b} \frac{f_{mn}}{\lambda_{mn} K_{mn}} \frac{m^2 \pi^2 v^2}{a^2} \operatorname{Sin} \frac{m\pi v t}{a}, \tag{12}$$

$$m = 1, 2 \ldots, \qquad n = 1, 2 \ldots$$

The solution of this set of equations is quite straightforward and can be completed if the initial conditions are known. In this paper, the bridge will be considered to be at rest initially. Accordingly,

$$W(x, y, 0) = 0 \tag{13a}$$

and $$\frac{\partial W}{\partial t}(x, y, 0) = 0. \tag{13b}$$

These equations lead to the relations,

$$U(x,y,0) = -\overline{W}(x,y,0)$$

and
$$\frac{\partial U}{\partial t}(x,y,0) = -\frac{\partial \overline{W}}{\partial t}(x,y,0)$$

or,
$$q_{mn}(0) = 0 \quad \text{and} \quad \dot{q}_{mn}(0) = -\frac{Pa^2}{D_x}\frac{a}{b}\frac{f_{mn}}{\lambda_{mn}K_{mn}}\alpha_m,$$

where
$$\alpha_m = \frac{m\pi v}{a}.$$

The solution of (12) can now be finally expressed as,

$$q_{mn}(t) = \frac{Pa^2}{D_x}\frac{a}{b}\frac{f_{mn}}{\lambda_{mn}K_{mn}}\frac{\alpha_m^2}{(p_{mn}^2-\alpha_m^2)}\left\{\operatorname{Sin}\alpha_m t - \frac{p_{mn}}{\alpha_m}\operatorname{Sin}p_{mn}t\right\} \tag{14}$$

Computation of Amplification Factors

From (2), it follows that

$$W = \frac{Pa^2}{D_x}\left[\delta_D + \frac{a}{b}\sum_{m=1,\ldots}^{\infty}\sum_{n=1,\ldots}^{\infty}\frac{f_{mn}}{\lambda_{mn}K_{mn}}Y_{mn}\operatorname{Sin}\frac{m\pi x}{a}\frac{\alpha_m^2}{(p_{mn}^2-\alpha_m^2)}\right.$$
$$\left.\cdot\left\{\operatorname{Sin}\alpha_m t - \frac{p_{mn}}{\alpha_m}\operatorname{Sin}p_{mn}t\right\}\right], \tag{15}$$

where
$$\delta_D = \frac{a}{b}\sum_{m=1,\ldots}^{\infty}\sum_{n=1,\ldots}^{\infty}\frac{f_{mn}}{\lambda_{mn}K_{mn}}\operatorname{Sin}\alpha_m t\, Y_{mn}\operatorname{Sin}\frac{m\pi x}{a}. \tag{16}$$

δ_D can be computed by summing the series in (16). Since the speed does not influence the values of δ_D directly, the values can be obtained for closely spaced load positions after setting $vt = d$. The resulting influence line can be used to compute the values of δ_D for any load position by interpolation, irrespective of the speed of the moving force. The dynamic amplification factor for deflection may now be defined as

$$AFD = \frac{W D_x}{Pa^2(\delta_D)_{max}}. \tag{17}$$

The expression for the moment amplification factor may be deduced in a similar manner.

Now,
$$M_x = -D_x\frac{\partial^2 W}{\partial x^2}$$

neglecting the Poisson's ratio effect.

Hence,
$$M_x = P\left[\delta_M + \frac{a}{b}\sum_{m=1,\ldots}^{\infty}\sum_{n=1,\ldots}^{\infty}\frac{f_{mn}}{\lambda_{mn}K_{mn}}\frac{\alpha_m^2 m^2\pi^2}{(p_{mn}^2-\alpha_m^2)}\right.$$
$$\left.\cdot\left\{\operatorname{Sin}\alpha_m t - \frac{p_{mn}}{\alpha_m}\operatorname{Sin}p_{mn}t\right\}Y_{mn}\operatorname{Sin}\frac{m\pi x}{a}\right], \tag{18}$$

where $$\delta_M = \frac{a}{b} \sum_{m=1,\ldots}^{\infty} \sum_{n=1,\ldots}^{\infty} \frac{f_{mn}}{\lambda_{mn} K_{mn}} \operatorname{Sin} \alpha_m t \, m^2 \pi^2 Y_{mn} \operatorname{Sin} \frac{m \pi x}{a}. \tag{19}$$

The computation of δ_M can be carried out for various load positions irrespective of the speed of the moving force. The amplification factor for M_x now takes the form,

$$AFM = \frac{M_x}{P(\delta_M)_{max}}. \tag{20}$$

The computation of the maximum amplification factors for deflection and moment requires the values of W_{max} and $M_{x\,max}$. These are to be obtained from the expressions (15) and (18) respectively. To this end, the deflection and moment are calculated at closely spaced values of "t" and the maximum values are picked out from the history curves so obtained.

Numerical Studies

The values of the amplification factors for deflection and moment can be computed by considering a suitable number of terms in the series (15) and (18). The results of the numerical studies are presented in two forms — (a) The amplification spectra and (b) The history curves. The amplification spectra are the plots of maximum amplifications of deflection and moment against the speed parameter. The speed parameter may be defined as $\alpha = \frac{vT}{2a}$ where "v" is the speed of the force and T is the fundamental period of the bridge. The history curves reveal the time variation of the bridge deflection and moment at a particular point as the force crosses the bridge with a definite speed.

The most important variable besides the speed parameter, is the transverse position of the moving force. In this study, two values of the transverse position are considered by taking $c = 0.45\,b$ and $c = 0.0$. The former corresponds to the eccentrically loaded case and the latter to the concentrically loaded case. It is not feasible to consider $c = 0.5\,b$ for the eccentric loading since the force is considered to be distributed over a finite area. In all the computations e/b is taken to be 0.05.

The values of δ_D and δ_M are first computed for fixed locations of the moving force. The values of these coefficients for any position of the moving force may then be found by interpolation. The determination of the dynamic deflection and the moment now requires the summation of series in (15) and (18). This may be carried out by considering a finite number of terms depending on the rapidity of convergence of the series. The time variation of the deflection and moment at any point in the bridge has to be studied by selecting a definite time interval. This interval naturally depends on the highest frequency appearing in the series. In what follows, the computation has been carried out

by selecting the time interval to be one-tenth the period of the highest mode considered. The maximum values of the deflection and the moment can also be picked out while studying the time variation of these quantities. These values may then be used to compute the maximum amplification factors.

The results of the various numerical studies are presented in the following sections. The entire procedure has been programmed in Fortran to work on the CDC-3600 computer at the Tata Institute of Fundamental Research, Bombay. The dynamic deflection and moment have been computed only for points at midspan. Five points at midspan have been considered: $y = \pm 0.45\,b$; $y = \pm 0.225\,b$ and $y = 0.0$. All the dynamic quantities are presented as ratios of the maximum static effects at the point under study.

Two typical Highway bridges are considered for detailed numerical investigation. The dimensions and the properties of the two bridges are presented in Table A.

Table A. Details of bridges considered

No.	Bridge Type	Span	a/b	D_x/D_y	$H/\sqrt{D_x D_y}$	$\sqrt{D_x}$ (kg·m)$^{1/2}$	ρ kg·sec^2/m^3
1	Slab	5 m	1.0	1.0	1.0	2500.0	60.0
2	Beam and Slab	20 m	2.0	100.0	0.4	25000.0	90.0

It is believed that the two bridges are representative of a good majority of Highway bridges where two-dimensional effects are prominent.

Convergence of the Solution

The convergence of the series in (15) and (18) are studied by considering different number of terms. The time histories for AFD and AFM for various number of terms considered are presented in Figs. 2 to 5. In all these figures a maximum of three modes are considered and the highest mode corresponds to $m = 1$ and $n = 3$. The solutions by considering lesser number of terms are also plotted to study the convergence.

Fig. 2 shows the behaviour of AFD for the beam and slab bridge under eccentric loading, the speed parameter being 0.193. The figure shows that the difference between the 2-mode solution and the 3-mode solution is small. The solutions for four modes and five modes were also computed and the resulting AFD's were found to coincide with the 3-mode solution on the graph. The figure also shows that the substantial component of the response consists of the first three modes of vibration of the bridge.

Fig. 3 shows the variation of AFM for the beam and slab bridge under eccentric loading. The speed parameter is again equal to 0.193. The con-

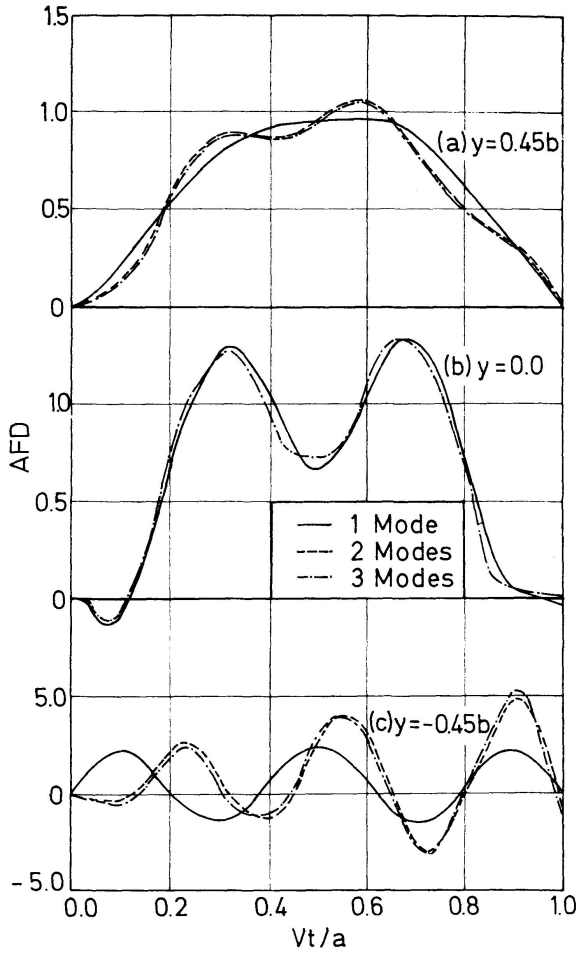

Fig. 2. Influence of various modes on the midspan deflection in the beam and slab bridge.
Force along $y = 0.45\ b$; $\alpha = 0.193$.

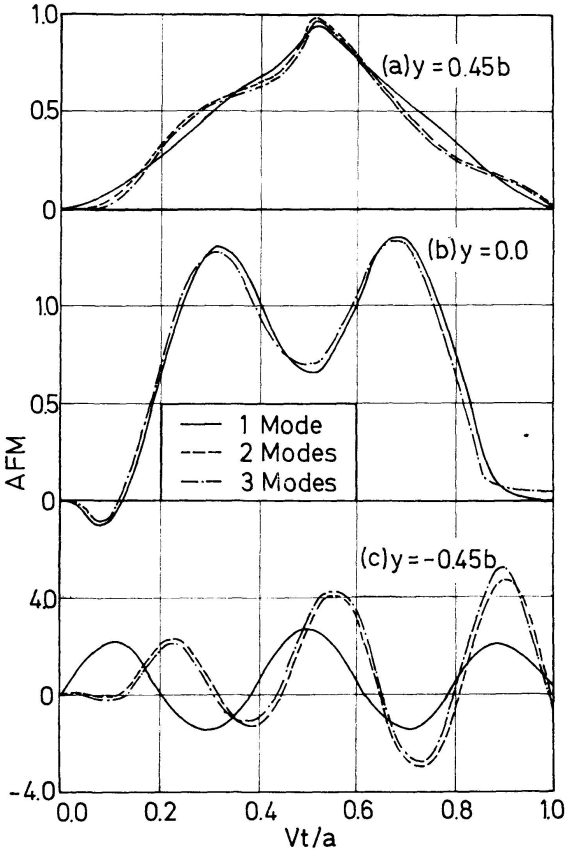

Fig. 3. Influence of various modes on the midspan moment (M_x) in the beam and slab bridge.
Force along $y = 0.45$; $\alpha = 0.193$.

vergence of the dynamic moment is seen to be quite satisfactory. Consideration of higher modes did not cause any appreciable change in the values of AFM and the first three modes may be considered to dominate the response. Fig. 4 shows the AFM variation for the beam and slab bridge under concentric loading. Because of the concentric loading, the second mode does not participate in the response and only the first mode and the third mode affect the moment and deflection values. The convergence of the values is again seen to be satisfactory with the first three modes. Consideration of more terms did not lead to any change in the graphs presented in Fig. 4.

Fig. 5 shows the behaviour of AFM for the slab bridge under eccentric loading, the speed parameter being 0.197. The consideration of modes more than three again did not introduce any noticeable changes in the history curves. Although the Figs. 4 and 5 consider the convergence of AFM, the convergence for AFD for the same cases was also found to be quite satisfactory. Comparison of the two series in (15) and (18) shows that the terms

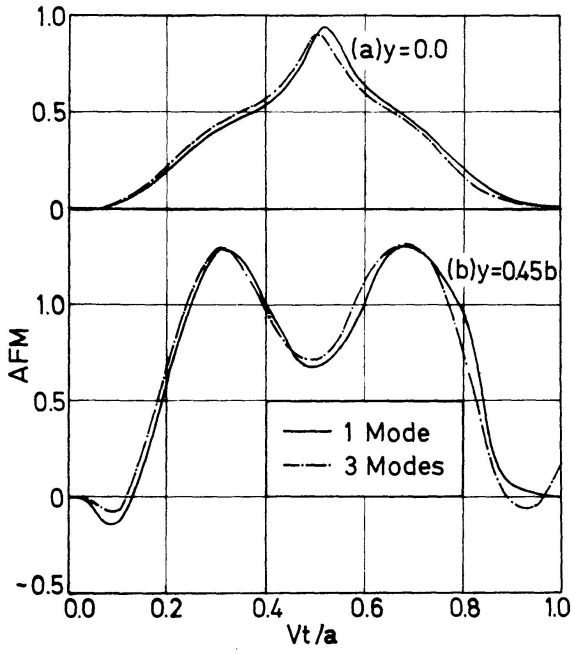

Fig. 4. Influence of various modes on the midspan moment (M_x) in the beam and slab bridge.
Force along $y = 0.0$; $\alpha = 0.193$.

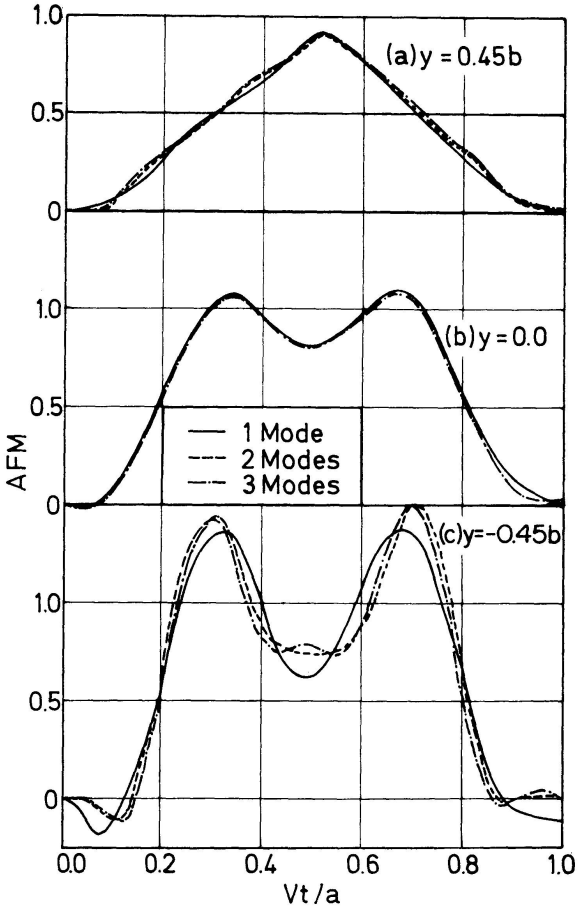

Fig. 5. Influence of various modes on the midspan moment (M_x) in the slab bridge.
Force along $y = 0.45\ b$; $\alpha = 0.197$.

are practically identical and the same rapidity of convergence may be expected for both AFM and AFD.

The convergence studies made in the above considered only terms with $m = 1$. Some sample calculations were made including the term corresponding to $m = 3$ and $n = 1$. It was found that the addition of this term did not alter any of the history curves presented. The influence of modes with m greater than unity may therefore be safely neglected for the midspan response. Modes with $m = 2$ need not be considered for midspan response as such modes will have a nodal line at the midspan. These modes would be of importance while considering the response of points away from the midspan.

The Amplification Spectra

The maximum dynamic amplification of any response quantity of the bridge under a moving force may be conveniently studied by drawing spectral curves. In this study the maximum amplification factors for deflection and

moment (M_x) at midspan are plotted against the speed parameter α. Three points at midspan are considered: $y = \pm 0.45b$ and $y = 0.0$. The spectra are drawn for (a) the eccentrically loaded case ($c = 0.45b$) and (b) the concentrically loaded case ($c = 0.0$). The slab bridge and the beam and slab bridge considered earlier are analysed for the spectral curves. All the computations are made taking 5 modes ($m = 1$ for all modes) into consideration.

The spectra are presented in Figs. 6 to 9. Figs. 6 and 7 refer to the concentric loading of the slab bridge and the beam and slab bridge respectively. In each figure, the spectral curves by the simple beam theory are also inserted for comparison. The two figures show that the amplification factors for $y = 0$ and $x = a/2$ in concentrically loaded bridges follow much the same pattern found in the midspan of a beam. The amplifications of $y = 0$ and $x = a/2$ in the two bridges are somewhat lesser in magnitude than the amplifications at the midspan of a beam. The amplification factors are larger at the edges than at $y = 0$ and $x = a/2$. The $(AFM)_{max}$ and $(AFD)_{max}$ values at the edges are practically identical in both the bridges. The amplifications at the edges of the beam and slab bridge are quite large and reach values of the order of 1.5 for the higher speeds.

Figs. 8 and 9 show the $(AFM)_{max}$ and $(AFD)_{max}$ values in the slab bridge and the beam and slab bridge respectively, due to eccentric loading. The amplification factors at the loaded edge ($y = 0.45b$) do not closely follow the

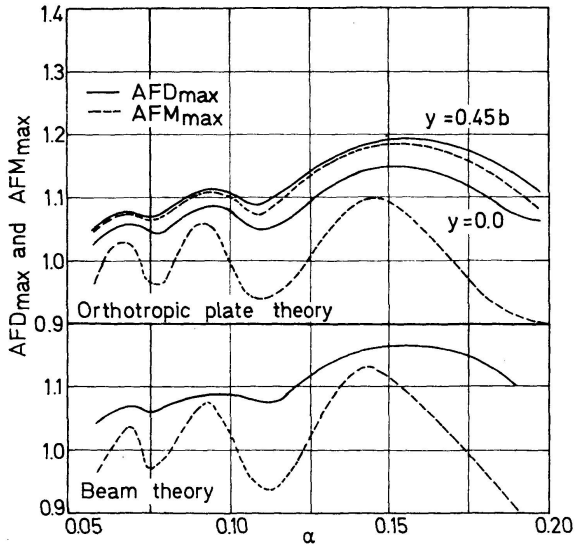

Fig. 6. Amplification spectra for the slab bridge with concentric moving force. Force along $y = 0.0$.

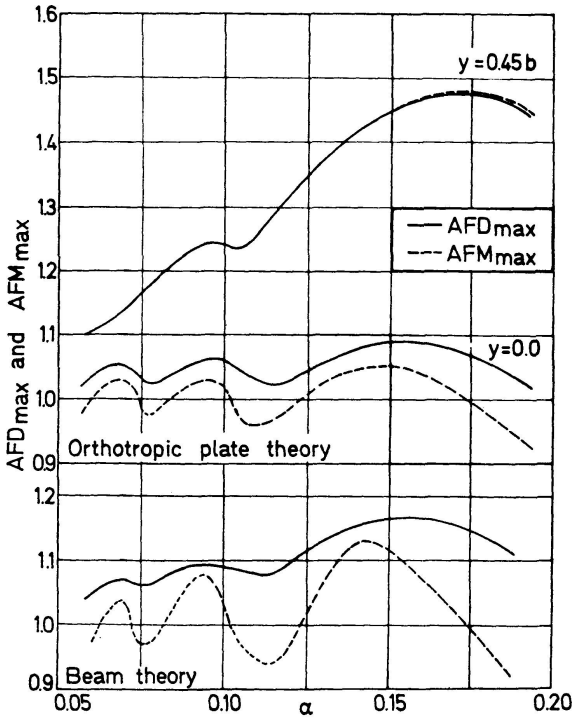

Fig. 7. Amplification spectra for the beam and slab bridge with concentric moving force. Force along $y = 0.0$.

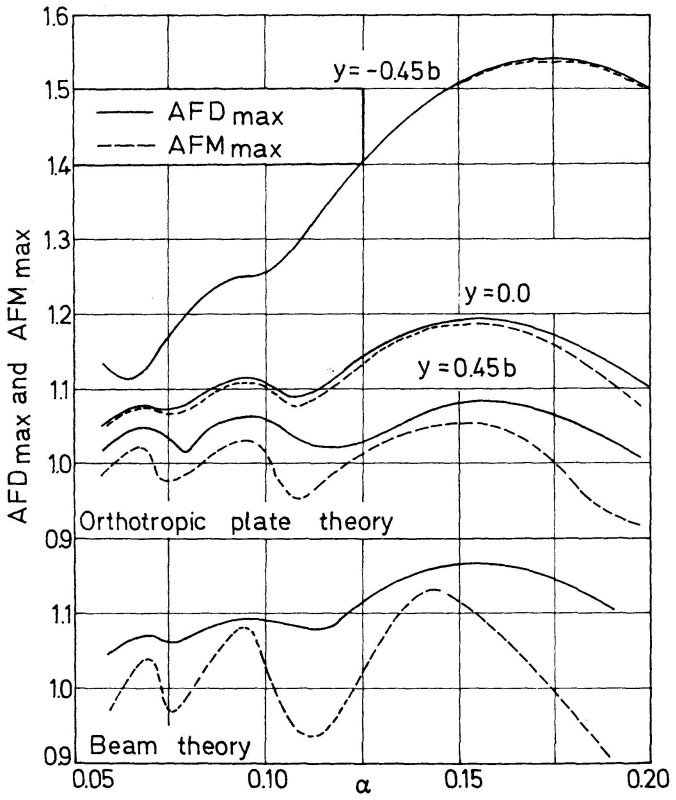

Fig. 8. Amplification spectra for the slab bridge with eccentric moving force.
Force along $y = 0.45\ b$.

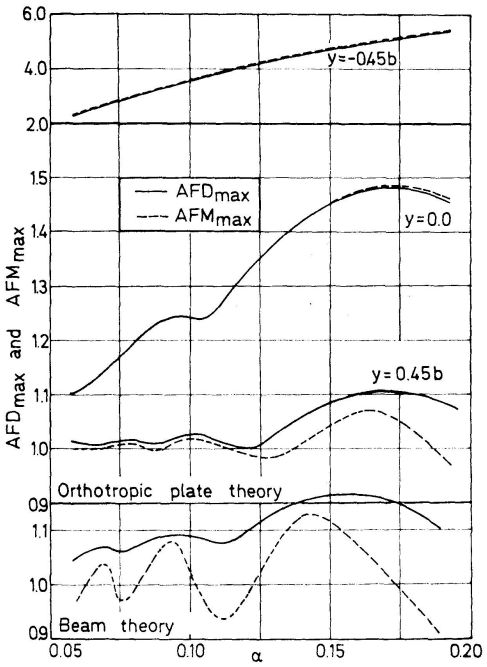

Fig. 9. Amplification spectra for the beam and slab bridge with eccentric moving force.
Force along $y = 0.45\ b$.

pattern found in beams. The disparity between the beam theory and the two-dimensional theory is greater for the beam and slab bridge. The unloaded edge ($y = -0.45b$) experiences quite large amplifications. There are considerable differences between the behaviour of the slab bridge and the beam and slab bridge with reference to the response of the unloaded edge. The beam and slab bridge shows pronounced oscillations at the unloaded edge in contrast to the slab bridge.

When the beam and slab bridge is subjected to eccentric loading, the unloaded edge experiences amplifications of the order of 5.0 for the higher speeds of the moving force.

The Transverse Distribution of Dynamic Effects

Fig. 10 shows the profile variation of the midspan deflection and moment in the beam and slab bridge as the force moves along, the speed parameter being 0.193. The figure refers to concentric loading ($c = 0.0$). The dynamic profiles are plotted in bold lines for various positions of the force along the

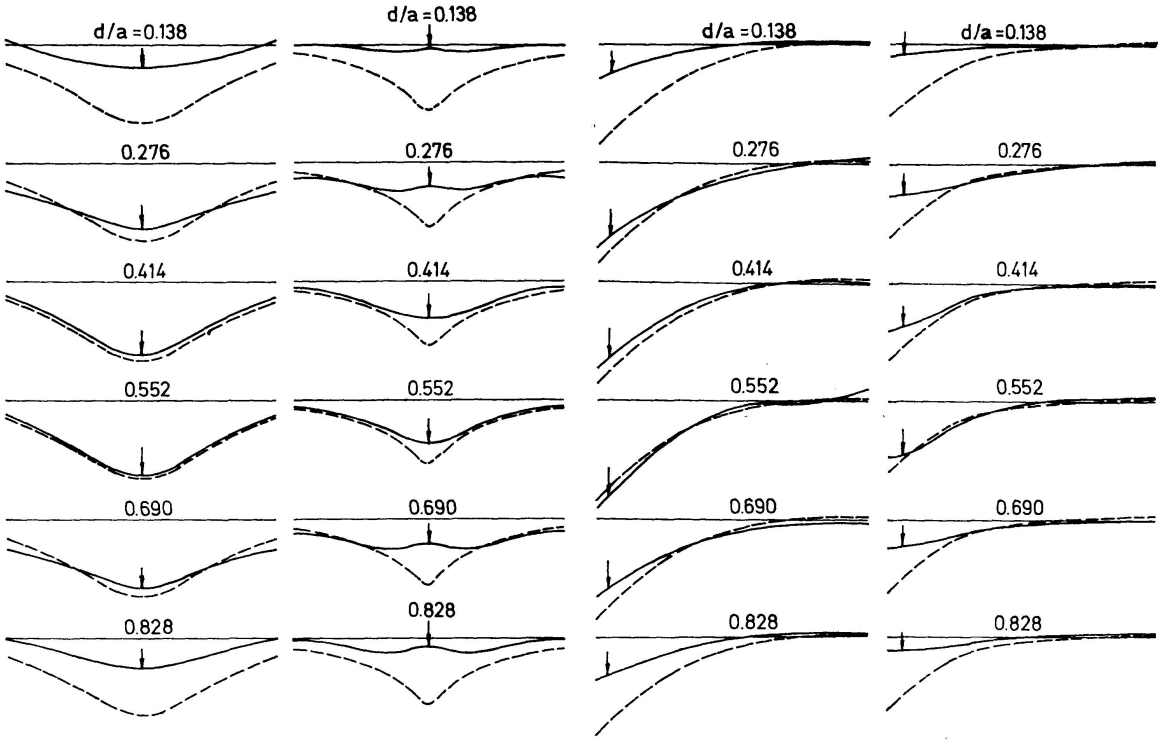

Fig. 10. Transverse distribution of dynamic deflection and moment at midspan of the beam and slab bridge.
Force along $y = 0.0$; $\alpha = 0.193$.

Fig. 11. Transverse distribution of dynamic deflection and moment at midspan of the beam and slab bridge.
Force along $y = 0.45\,b$; $\alpha = 0.193$.

bridge. The static deflection profile at midspan, when the force is also at midspan, is shown in dotted lines along with each profile sketch.

The dynamic deflection profile is seen to be dominated by the contribution of the fundamental and the second symmetric modes. The change in the profile as the force moves from $d = 0.552\,a$ to $d = 0.69\,a$ clearly indicates the participation of the second symmetric mode. Fig. 10b) shows the dynamic moment variation (M_x) at midspan. Unlike the maximum static moment at midspan, the dynamic moment is more uniformly distributed across the width of the bridge. This may be attributed to the distributing effect of the inertia forces of the bridge.

Fig. 11a) shows the midspan deflection profile of the beam and slab bridge as the force moves eccentrically along $y = +0.45\,b$. The speed parameter is again 0.193. The participation of the various modes is more complex in eccentric loading than what is found in concentric loading. Fig. 11b) shows the midspan moment (M_x) variation across the width for eccentric loading of the beam and slab bridge. The dynamic distribution of the deflection and the moment M_x are both seen to be more uniform than the maximum static profiles.

History Curves

The history curve for any response quantity shows the quantity as a function of time as the force crosses the bridge. Some typical history curves for the deflection and moment at midspan of the two bridges are presented here.

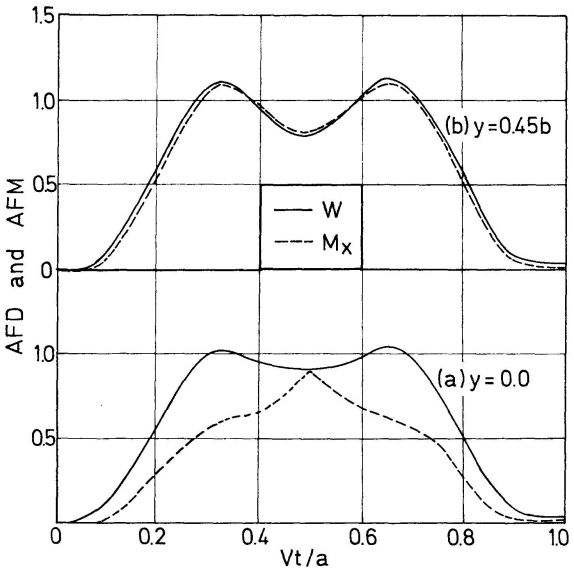

Fig. 12. History curves for the midspan deflection and moment amplifications in the slab bridge.
Force along $y = 0.0$; $\alpha = 0.197$.

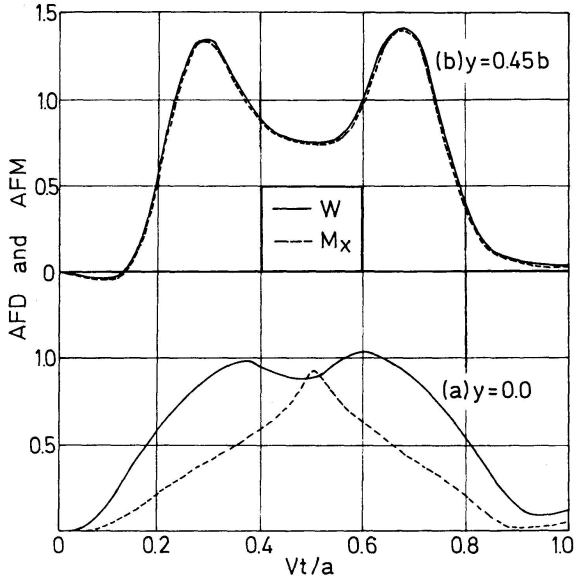

Fig. 13. History curves for the midspan deflection and moment amplifications in the beam and slab bridge.
Force along $y = 0.0$; $\alpha = 0.193$.

Figs. 12 and 13 show the history curves for the slab bridge and the beam and slab bridge respectively, when the moving force is concentric. The speed parameter is 0.197 for the slab bridge and 0.193 for the beam and slab bridge. There are considerable differences between the moment (M_x) and deflection curves for $y = 0.0$. This may be attributed to the differences between the static influence lines for the two quantities. The influence line for M_x at $y = 0$ and $x = 0.5\,a$ has a very sharp peak at the centre. The deflection influence line for the same point happens to be a much smoother curve. Even after adding the inertia effects, the differences between the time variation of the two quantities show up in the history curves. It is also seen that the maximum dynamic moment for $y = 0.0$ occurs when the force is very close to midspan if not at the midspan. The maximum dynamic deflection at $y = 0.0$ may occur even when the force is well removed from midspan. The situation is somewhat different for midspan points at $y = \pm 0.45\,b$, wherein the moment and deflection amplifications follow each other very closely. In contrast to the point $y = 0.0$, the inertia effects are comparable to the static effects at the points $y = \pm 0.45\,b$.

Figs. 14 to 16 show the history curves for eccentrically loaded bridges. Fig. 14 refers to the slab bridge subjected to an eccentric moving force, the

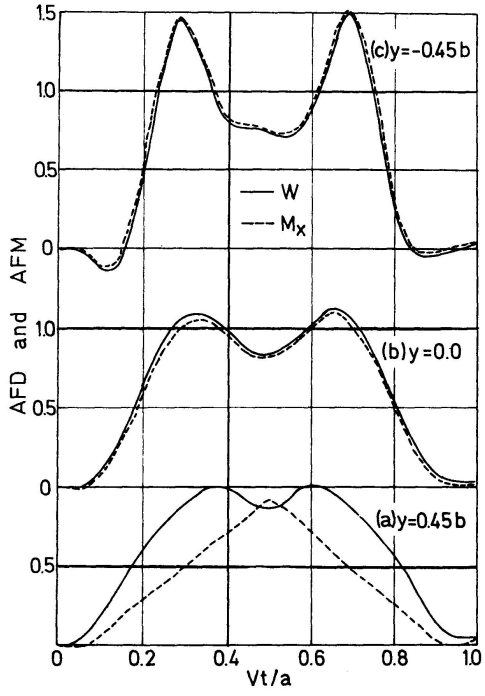

Fig. 14. History curves for the midspan deflection and moment amplifications in the slab bridge. Force along $y = 0.45\,b$; $\alpha = 0.197$.

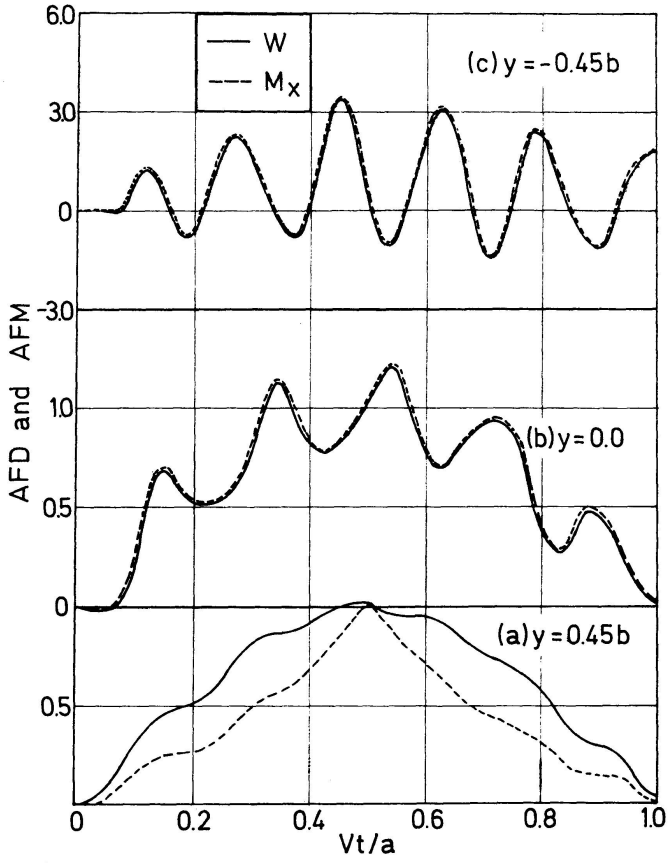

Fig. 15. History curves for midspan deflection and moment amplifications in the beam and slab bridge. Force along $y = 0.45b$; $\alpha = 0.097$.

speed parameter being 0.197. Figs. 15 and 16 refer to the beam and slab bridge under eccentric moving force, the speed parameter values being 0.097 and 0.193 respectively. The history curves for $y = +0.45\,b$ and $x = 0.5\,a$ follow much the same trend followed by the curves for the midspan point at $y = 0.0$ in the case of concentric loading. The inertia effects dominate the response as points farther away from the line of loading are considered. This is especially true for the beam and slab bridge, where the edge $y = -0.45\,b$ reveals an interesting feature. The point at midspan of this bridge corresponding to $y = -0.45\,b$, executes a beating type motion as the force moves along the edge $y = +0.45\,b$. The dynamic effects in this case are far in excess of the static response values. Large amplifications are obtained and the maximum amplification may occur when the force is nearing the support $x = a$ (Fig. 16). This beat phenomenon is observed for both the values of the speed parameter ($\alpha = 0.097$ and 0.193) considered in Figs. 15 and 16. This behaviour may be directly attributed to the frequency distribution existing in the beam and slab bridge. In Table B the frequencies of the two bridges described in Table A, are tabulated. The Table shows that the first two frequencies of the beam and slab bridge are quite close. This closeness of the frequencies causes the

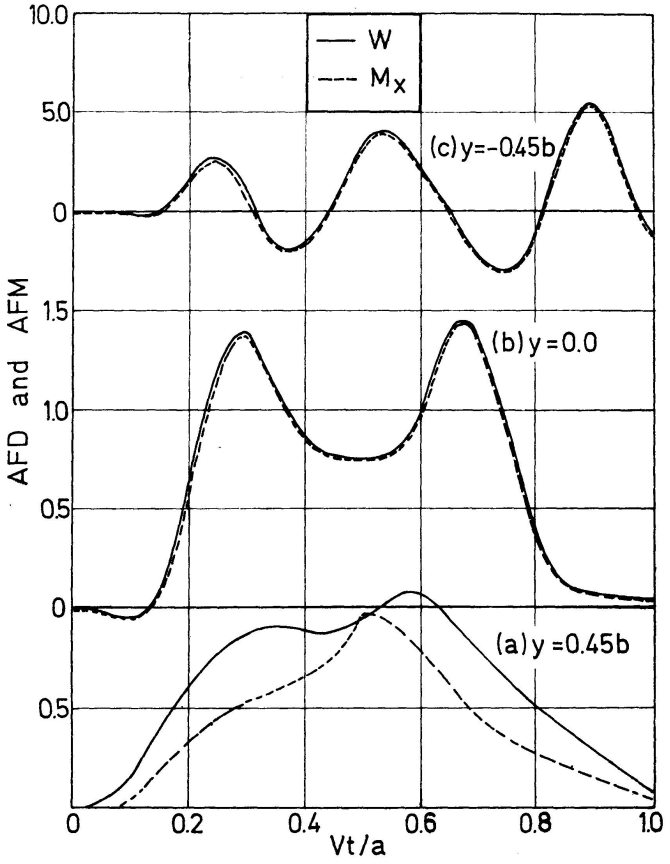

Fig. 16. History curves for midspan deflection and moment amplifications in the beam and slab bridge. Force along $y = 0.45b$; $\alpha = 0.193$.

beat type phenomenon at the unloaded edge. The frequencies of the slab bridge are quite sparsely distributed and the unloaded edge of this bridge does not show the beating motion for eccentric loading.

Table B. Frequencies of the bridges

Type	Frequencies in c/s ($m = 1$ for all modes)			
	Fundamental	I Asymmetric	II Symmetric	II Asymmetric
Slab	20.27	36.73	80.57	159.3
Beam and Slab	10.34	12.09	18.98	33.88

Conclusions

Some general conclusions may be drawn from the results obtained for the two typical bridges. The conclusions may be summarised as follows:

a) The midspan response of the Highway bridge is influenced mostly by the first three modes of vibration. Although this conclusion has been drawn with

reference to two bridges, it may be extended to other bridges where the frequencies of the first three modes are clustered together. It has been shown by SUNDARA RAJA IYENGAR, JAGADISH and NARAYANA IYENGAR [7] that the frequencies of most of the Highway bridges follow this pattern.

b) When a bridge is subjected to a concentric moving force, the amplification factors for points below the moving force follow the trend found in beams. The values of the amplifications found by the orthotropic plate theory are smaller than the values found by the beam theory. When the bridge is under eccentric moving force, the amplifications for points below the moving force do not closely follow the trend found in beams.

c) For a point underneath the moving force the maximum moment occurs when the force is at the point or very close to it. The maximum deflection at the point can occur even when the force has moved away from the point.

d) The maximum amplification increases as points away from the line of loading are considered. The largest amplifications are realised at the unloaded edge of a bridge under eccentric loading. This effect is more pronounced in the beam and slab bridge than in the slab bridge. If the first two frequencies of a bridge are very close, the unloaded edge executes a beating type motion, when the bridge is under eccentric moving force.

Notations

AFD	Amplification factor for deflection
AFM	Amplification factor for moment
a	Span of the bridge
b	Width of the bridge
c	y-co-ordinate of the moving force
$d = v\,t$	x-co-ordinate of the moving force at any instant
D_x, D_y, H_{xy}	Orthotropic plate constants
e	Half the side of the square distributing the force over the bridge surface
p_{mn}	Circular frequency of the orthotropic plate
U	Inertia force solution
v	Speed of the force
W	Dynamic deflection of the plate
$\overline{W}$	Crawl solution
α_{mn}, β_{mn}	Parameters in the plate characteristic function
$\alpha_m = \frac{m\pi v}{a}$	Crossing frequency
$\alpha = \frac{vT}{2a}$	Speed parameter
δ_D, δ_M	Influence coefficients for static deflection and moment
λ_{mn}	Frequency parameter
ρ	Mass per unit area of the orthotropic plate

Appendix

The expressions for $Y_{mn}(y)$ are presented in this appendix. The functions $Y_{mn}\,\mathrm{Sin}\frac{m\pi x}{a}$ happen to be the shape functions of an orthotropic plate with two opposite edges simply-supported and the other two free. The expressions for the functions may be easily obtained by a free-vibration analysis of the plate.

Modes symmetric in $y-n$ is odd

(I) $D_1 \neq 0$,

$$Y_{mn}(y) = \frac{\mathrm{Cosh}\frac{\alpha_{mn}y}{b}}{\mathrm{Cosh}\frac{\alpha_{mn}}{2}} + \frac{\alpha_{mn}^2 - \frac{D_1}{D_y}\frac{m^2\pi^2b^2}{a^2}}{\beta_{mn}^2 + \frac{D_1}{D_y}\frac{m^2\pi^2b^2}{a^2}} \frac{\mathrm{Cos}\frac{\beta_{mn}y}{b}}{\mathrm{Cos}\frac{\beta_{mn}}{2}}.$$

where α_{mn} and β_{mn} satisfy the equations,

$$\tan\frac{\beta_{mn}}{2} = -\frac{\alpha_{mn}}{\beta_{mn}}\left[\frac{\beta_{mn}^2 + \frac{D_1}{D_y}\frac{m^2\pi^2b^2}{a^2}}{\alpha_{mn}^2 - \frac{D_1}{D_y}\frac{m^2\pi^2b^2}{a^2}}\right]^2 \tanh\frac{\alpha_{mn}}{2}$$

and

$$\alpha_{mn}^2 = \frac{2H_{xy}}{D_y}\frac{m^2\pi^2b^2}{a^2} + \beta_{mn}^2.$$

(II) $D_1 = 0$,

$$Y_{m1}(y) = 1$$

and

$$\beta_{m1} = 0.$$

For values of n greater than unity, expressions of (I) may be used.

Modes antisymmetric in $y-n$ is even

$$Y_{mn}(y) = \frac{\mathrm{Sinh}\frac{\alpha_{mn}y}{b}}{\mathrm{Sinh}\frac{\alpha_{mn}}{2}} + \left[\frac{\alpha_{mn}^2 - \frac{D_1}{D_y}\frac{m^2\pi^2b^2}{a^2}}{\beta_{mn}^2 + \frac{D_1}{D_y}\frac{m^2\pi^2b^2}{a^2}}\right]\frac{\mathrm{Sin}\frac{\beta_{mn}y}{b}}{\mathrm{Sin}\frac{\beta_{mn}}{2}},$$

where α_{mn} and β_{mn} satisfy the equations,

$$\tan\frac{\beta_{mn}}{2} = \frac{\beta_{mn}}{\alpha_{mn}}\left[\frac{\alpha_{mn}^2 - \frac{D_1}{D_y}\frac{m^2\pi^2b^2}{a^2}}{\beta_{mn}^2 + \frac{D_1}{D_y}\frac{m^2\pi^2b^2}{a^2}}\right]^2 \tanh\frac{\alpha_{mn}}{2}$$

and

$$\alpha_{mn}^2 = \frac{2H_{xy}}{D_y}\frac{m^2\pi^2b^2}{a^2} + \beta_{mn}^2.$$

References

1. J. P. Alfaro and A. S. Veletsos: "Dynamic behaviour of an I-Beam Bridge Model Under a Smoothly Rolling Load". Civil Engineering Studies, Structural Research Series No. 167, University of Illinois, 1958.
2. C. Oran and A. S. Veletsos: "Analysis of Static and Dynamic Response of Simple-Span, Multigirder Highway Bridges". Civil Engineering Studies, Structural Research Series No. 221, University of Illinois, 1961.
3. G. M. Foster and L. T. Oehler: "Vibrations and deflections of Rolled-beam and Plate-Girder Bridges". Highway Research Board Bulletin 124, National Academy of Science, Washington D.C., 1956.
4. L. T. Oehler: "Vibration Susceptibilities of various Highway Bridge Types". Proceedings of the American Society of Civil Engineers, Paper No. 1318, Vol. 83, ST 4, July 1957.
5. K. T. Sundara Raja Iyengar and R. Narayana Iyengar: "Free Vibration of Beam and Slab Bridges". Publ. IABSE, Vol. 27, 1967.
6. R. Narayana Iyengar: "Studies in the Free Vibration of Beam and Slab and Interconnected Girder Bridges". Thesis submitted for the degree of the Master of Science in Engineering, Indian Institute of Science, Bangalore, 1966.
7. K. T. Sundara Raja Iyengar, K. S. Jagadish and R. Narayana Iyengar: "Free Vibration of Beam and Slab Bridges". The Journal of the Institute of Engineers (India), Vol. XLVIII, No. 1, Pt CI 1, September 1967 (Special).

Summary

The dynamic response of simple-span beam and slab Highway bridges subjected to a moving concentrated force is studied. The Highway bridge is treated as an orthotropic plate, and the normal mode method is used in the response analysis. Numerical results are presented for typical cases in the form of amplification spectra and history curves.

Résumé

L'auteur étudie le comportement dynamique de ponts d'autoroute en dalle, à une seule ouverture, sous une force mobile concentrée. La méthode normale est employée pour l'analyse du comportement, le pont étant assimilé à une dalle orthotrope. Pour les cas-types, des valeurs numériques sont données sous forme de spectres amplificateurs et de courbes d'hystérésie.

Zusammenfassung

Der Autor behandelt das dynamische Verhalten von einfachen Platten- und Balkenbrücken für Autobahnen unter einer konzentrierten, beweglichen Kraft. Die Brücke wird als orthotrope Platte behandelt und die Rechenwerte mit der normalen Methode ermittelt. Für typische Fälle sind numerische Werte angegeben in der Form von Vergrößerungsspektren und Hysteresiskurven.